LETTER   **Open Access**

Tsunami-induced magnetic fields detected at Chichijima Island before the arrival of the 2011 Tohoku earthquake tsunami

Hidee Tatehata[1*], Hiroshi Ichihara[2,3] and Yozo Hamano[4]

Abstract

Magnetic field disturbances associated with the tsunami caused by the 2011 Tohoku earthquake were observed at Chichijima Island, 1200 km south of the epicenter. The vertical component of the magnetic field showed a periodic signal at approximately 20 min before the tsunami arrived. This study investigated the mechanism of the magnetic field signal using simulation studies. First, we derived a tsunami source model that explained the tide gauge records and sea-level changes at Chichijima Island. Using this model, we then computed the electric current induced by the tsunami and the resulting secondary magnetic field. The computed changes in sea level and magnetic field are consistent with their respective observed waveforms, including the timing of the magnetic field signals. In our interpretation, the tsunami flow induced an electric current along the tsunami wave front, which in turn generated a secondary induced magnetic field ahead of the tsunami wave. Hence, magnetic variations preceding the tsunami were observed at Chichijima Island. This suggests that imminent arrivals of tsunamis can be detected by observations of the magnetic field.

Findings

Introduction

The oceanic dynamo effect was anticipated theoretically by Michael Faraday (Faraday 1832) and has been studied in further detail during recent decades (e.g., Sanford 1971; Tyler 2005; Tyler et al. 2003). With the advancement of observational devices, tsunami-induced dynamo effects have recently been observed on the seafloor (Toh et al. 2011; Ichihara et al. 2013; Sugioka et al. 2014; Zhang et al. 2014a). A few instances of these effects have been documented on land. One was a magnetic signal associated with the 27 February 2010 earthquake (M8.8) off the coast of Chile, which was observed at Easter Island, 3500 km from the epicenter (Manoj 2011). A magnetic signal associated with the tsunami caused by the 11 March 2011 Tohoku earthquake (M9.0) was observed in Chichijima Island, from which a clear signal of the oceanic dynamo effect was reported by Zhang et al. (2014b). They reproduced the observed magnetic field

but did not perform a comparison between the tsunami and the magnetic field.

In this paper, we report on tsunami-induced magnetic field variations that were observed at Chichijima Island at approximately 20 min before the tide gauge there recorded the arrival of the tsunami.

The aims of this study were to confirm that the oceanic dynamo effect caused the magnetic field variations and to understand the mechanism that allowed the detection of the magnetic field variations before the sea-level change. In this paper, we first present and compare the sea-level changes and magnetic field variations after the 2011 Tohoku earthquake. Next, we report on our numerical simulations of tsunamis and induced magnetic fields at Chichijima Island to explain the corresponding observations. Finally, we discuss the mechanism by which the tsunami-induced magnetic field can signal a tsunami before the occurrence of changes in sea level.

* Correspondence: tatehata@met.kishou.go.jp
[1]Kakioka Magnetic Observatory, Japan Meteorological Agency, 595 Kakioka, Ishioka-shi, Ibaraki-ken 315-0116, Japan
Full list of author information is available at the end of the article

Tatehata *et al. Earth, Planets and Space* (2015) 67:185

Page 2 of 11

Observations at Chichijima Island

Tide gauge

Chichijima Island is situated on the Izu-Bonin-Mariana Ridge, about 1200 km south-southwest of the 2011 Tohoku tsunami source (Fig. 1). The tide gauge station, operated by the Japan Meteorological Agency (JMA), is on the northern side of Futami harbor and has an ultrasonic distance meter that measures sea-level changes at intervals of 15 s.
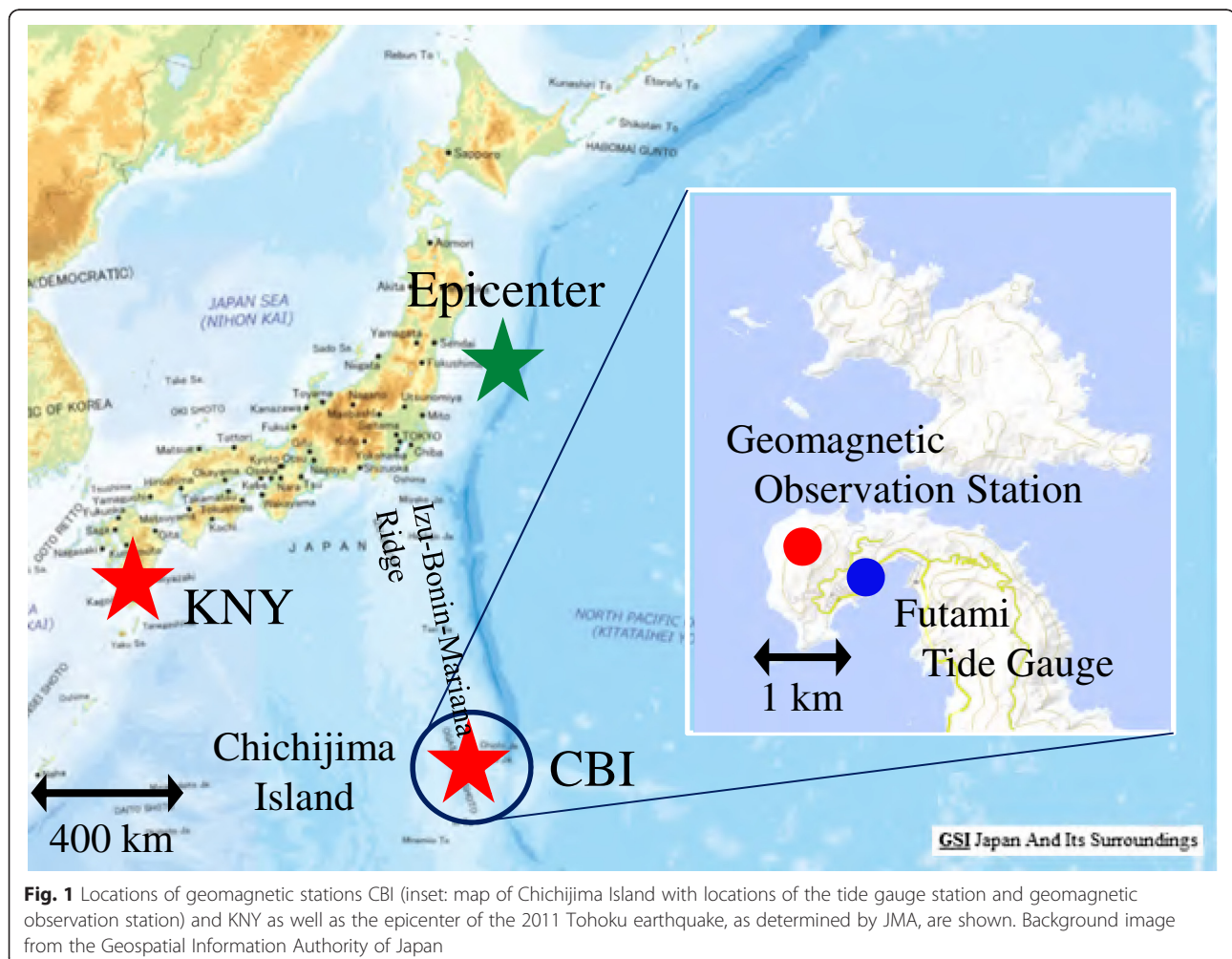
Magnetic observations

Magnetic field variations were observed at the Chichijima geomagnetic observation station (CBI), located 155 m above sea level on a hill approximately 1 km from the tide gauge station (Fig. 1). To compare the record of magnetic field variations with records from another site, we also used records from the Kanoya geomagnetic station (KNY) at the southern end of Kyushu Island, about 1000 km from Chichijima Island. Both observation stations are operated by the JMA and are equipped with fluxgate magnetometers with a resolution of 0.1 nT. Continuous time series of three magnetic components at an interval of 1 s are available from both stations (Fig. 2). We applied a band-pass digital filter (transmission period of 3–60 min) to remove diurnal variations and short-period instrumental noise.
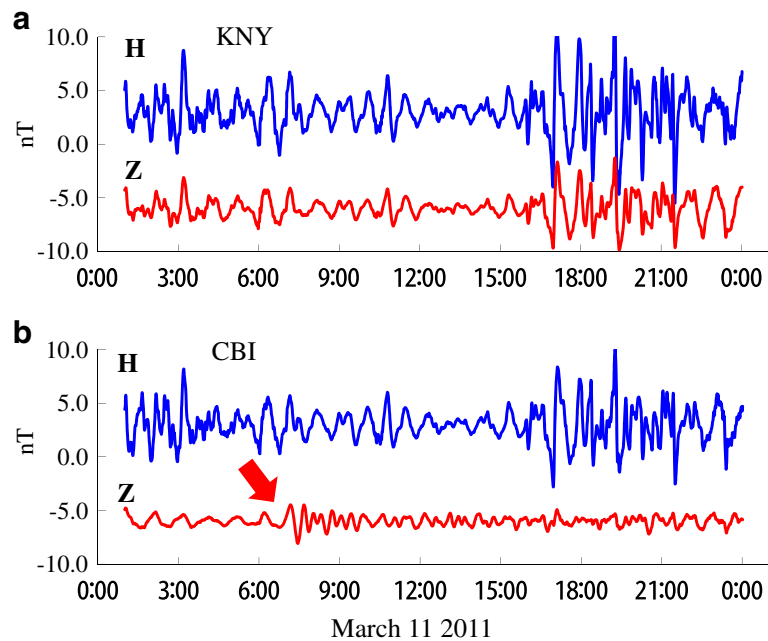
Figure 2 shows the horizontal component H and vertical component Z of the filtered geomagnetic records from CBI and KNY. Most of the simultaneous variations in these records are explained by a weak magnetic storm on 11 March 2011 (Japan Meteorological Agency 2013). However, the record of Z at CBI showed anomalous behavior starting around 7:00 (UTC) that could not be explained by the external source (see Appendix 1).

Comparison of tide gauge and magnetic records

Before comparing the magnetic and tidal records from Chichijima Island, they were band-pass filtered with a period of 3–60 min to remove diurnal and long-term signals. The resulting waveforms of sea-level change and the magnetic Z component were strikingly similar,

Fig. 1 Locations of geomagnetic stations CBI (inset: map of Chichijima Island with locations of the tide gauge station and geomagnetic observation station) and KNY as well as the epicenter of the 2011 Tohoku earthquake, as determined by JMA, are shown. Background image from the Geospatial Information Authority of Japan

Fig. 2 Magnetic field observations at **a** Kanoya (KNY) and **b** Chichijima (CBI). The *blue line* is the horizontal component *H* and the *red line* is the vertical component *Z*. The *red arrow* indicates the arrival of the anomalous signal associated with the tsunami

displaying seven sharp peaks between 7:00 and 9:30 (UTC) (Fig. 3).

Tidal records show that the tsunami arrived at 07:11 (UTC), with a maximum height (half amplitude) of 182 cm (Japan Meteorological Agency 2013). The dominant period of the tsunami between the first and seventh waves was around 20 min. The maximum amplitude of *Z*, observed in the second peak, was 1.6 nT. The predominant period of both waveforms was consistently about 20 min. The arrival times of the magnetic
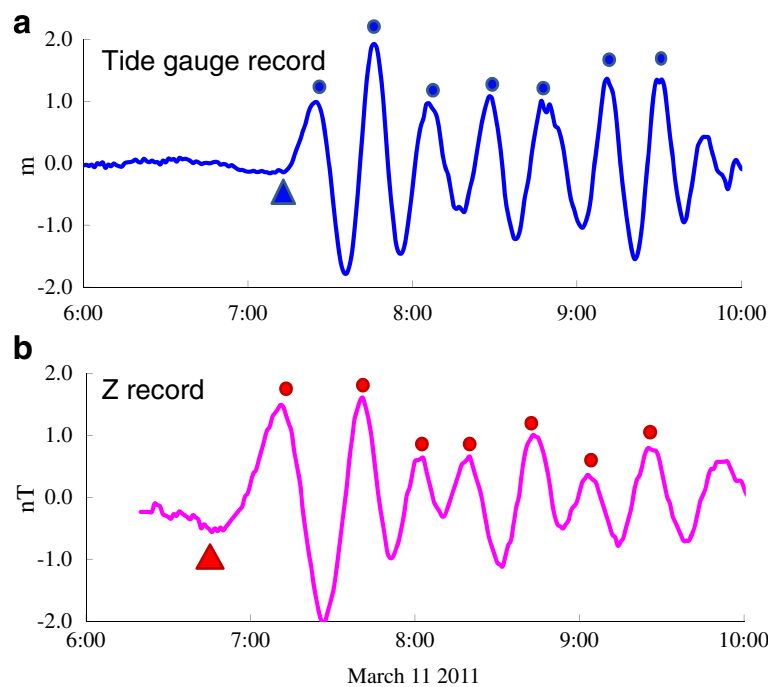
Fig. 3 a Tide gauge record and **b** *Z* record observed at Chichijima Island on 11 March 2011 (UTC). *Triangles* indicate the arrivals of the tsunami and the magnetic signal; peaks are indicated by *small circles*

Tatehata *et al. Earth, Planets and Space* (2015) 67:185

Page 4 of 11

signal were recorded at 06:50 showing that the initial magnetic signal preceded the initial tide gauge signal by about 20 min. The first peak of the magnetic signal preceded that of the tsunami wave by about 14 min, and the third through seventh magnetic peaks preceded those of the tsunami waves by about 5 min. For our purposes, the locations of the tidal and magnetic stations can be considered the same. Thus, the magnetic variations were detected 5–20 min ahead of the tsunami.

Simulations of tsunami flows and induced magnetic fields

We performed a numerical tsunami simulation that explains the tsunami observations at Chichijima Island and nearby offshore tide gauges. Then we computed the magnetic variation induced by the oceanic dynamo effect and compared the results to the magnetic observations. Our analysis involved three steps: first, computation of the flow of seawater in the simulation; second, computation of the electric current induced by seawater flow; and third, computation of the resulting magnetic field variations on the basis of the Biot-Savart law.

Tsunami flow model

Zhang et al. (2014b) studied the induced magnetic field at CBI through a numerical simulation. The amplitude of their computed magnetic waveform was slightly higher than that of the observation. They mentioned that the reason might be the low accuracy of the numerical tsunami simulation, which used a planar coordinate system.

We used a nonlinear numerical tsunami model that takes seabed friction and Coriolis force into consideration, where one grid size is 1 min of arc (along longitude and latitude), the time difference is 3.06 s, and the system of coordinates is spherical.

The computed and observed tsunami waveforms are shown in Fig. 4. Details of the tsunami model, earthquake fault parameters, and incorporation of data from buoys of Deep-ocean Assessment and Reporting of Tsunamis (DART) are presented in Appendix 2.

The computed waveform was sufficiently accurate considering the tsunami flow around Chichijima Island.

Induced electric current and magnetic field

The induction of electric currents from tsunami waves is depicted schematically in Fig. 5a. We computed the induced electric currents using the previously computed seawater flow. Ichihara et al. (2013) provided the theoretical details behind this computation.
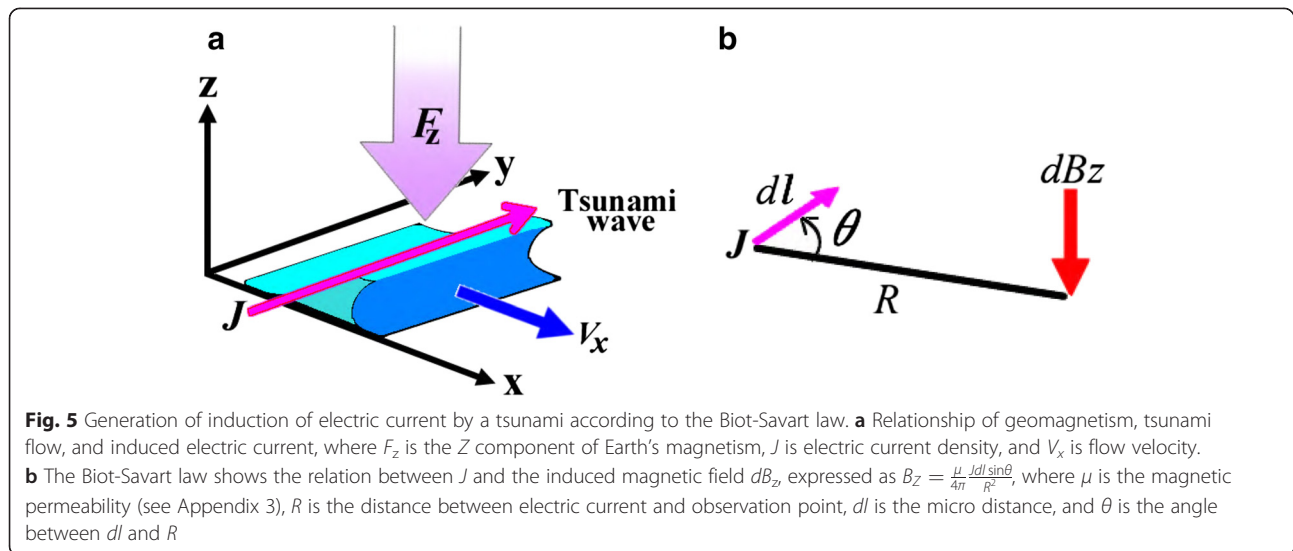
Tsunami waves could be approximated with sufficient accuracy by plane waves because the tsunami model described in the previous section used a small grid size of about 2×2 km. The electrical conductivity of seawater is assumed to be homogeneous in the vertical direction, and the electrical conductivities of the atmosphere and the seafloor are approximated at zero. The amplitude and phase shift of the induced current J are then derived using the following expression:

$$\mu J_\perp = -\frac{2i}{1-iC_d/C}\frac{\eta F_z}{h}, \tag{1}$$

where μ is the magnetic permeability, $J_\perp$ is the total electric current density in the direction perpendicular to the propagation of the tsunami, i is the imaginary unit, C_d is the magnetic diffusivity (the phase velocity of the electric current wave in seawater), C is the tsunami velocity, η is the tsunami height, F_z is the Z component of the geomagnetic field F, and h is the water depth. The imaginary unit represents the phase difference between the tsunami wave and the electric current in complex phase space. Details are presented in Appendix 3.
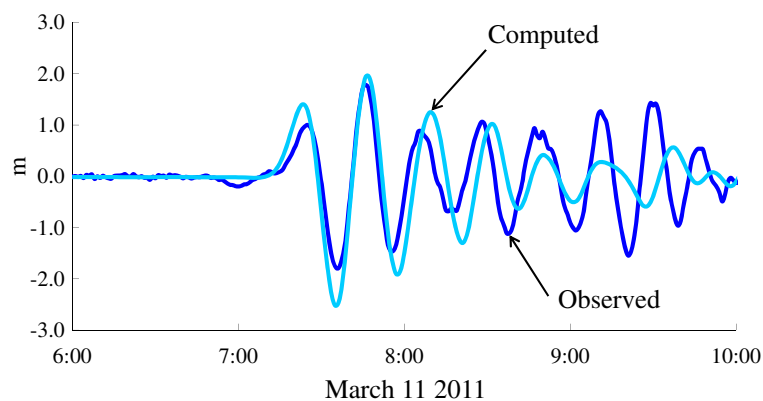
Fig. 4 Band-pass filtered tide gauge record from Chichijima Island showing observed tsunami waveforms (*dark blue*) and computed tsunami waveforms (*light blue*)

Tatehata *et al. Earth, Planets and Space* (2015) 67:185

Page 5 of 11

Fig. 5 Generation of induction of electric current by a tsunami according to the Biot-Savart law. **a** Relationship of geomagnetism, tsunami flow, and induced electric current, where F_z is the Z component of Earth's magnetism, J is electric current density, and V_x is flow velocity. **b** The Biot-Savart law shows the relation between J and the induced magnetic field dB_z, expressed as $B_Z = \frac{\mu}{4\pi} \frac{J dl \sin\theta}{R^2}$, where μ is the magnetic permeability (see Appendix 3), R is the distance between electric current and observation point, dl is the micro distance, and θ is the angle between dl and R
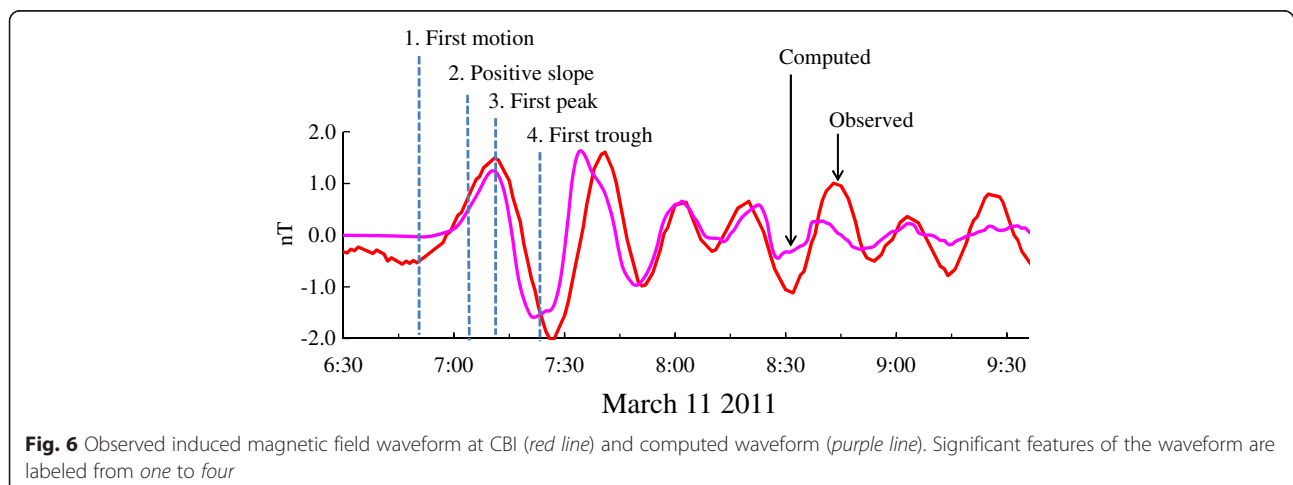
The specific computation steps are given below.

1. Time domain data of tsunami height for every numerical grid point are decomposed to frequency domain data by fast Fourier transform (FFT). The formula (1) converts the frequency domain data to electric currents in complex space. Inverse FFT is then used to convert the frequency domain data of the current to time domain data (in real space), expressed as the length of a current vector.
2. The flow direction of the tsunami is computed from the numerical tsunami model. According to Ampere's law, the electric current direction is obtained by rotated flow direction by 90°. The electric current density and its direction are then obtained for each grid cell.
3. The induced magnetic field at the observation point is computed from the induced current source in

each grid cell according to the Biot-Savart law (Fig. 5b). The induced magnetic field at CBI is obtained by integrating a sufficient area centered on Chichijima Island.

The computed and observed magnetic field variations at CBI are shown in Fig. 6. From the first motion to the fourth peak, the computed magnetic field agreed well with the observations. For the fifth and the seventh peaks, the amplitude of the computed waveform was reduced, but the timing of the peaks and troughs was consistent.

In sum, our computed sea-level changes and magnetic field variations agreed well with the observations, although we used only a simple electrical conductivity structure. This result indicates that the tsunami-induced magnetic field variations at Chichijima Island could be suitably computed by assuming an insulating seafloor.

Fig. 6 Observed induced magnetic field waveform at CBI (*red line*) and computed waveform (*purple line*). Significant features of the waveform are labeled from *one* to *four*

Tatehata *et al. Earth, Planets and Space* (2015) 67:185

Page 6 of 11

Discussion

To understand why the magnetic field variations preceded the sea-level changes at Chichijima Island, we compared the computed magnetic field variation to the patterns of seawater flow and induced electric currents around Chichijima Island (Fig. 7). Each distinctive phase from the first motion (6:53 UTC), the positive slope (7:05 UTC), the first peak (7:10 UTC),
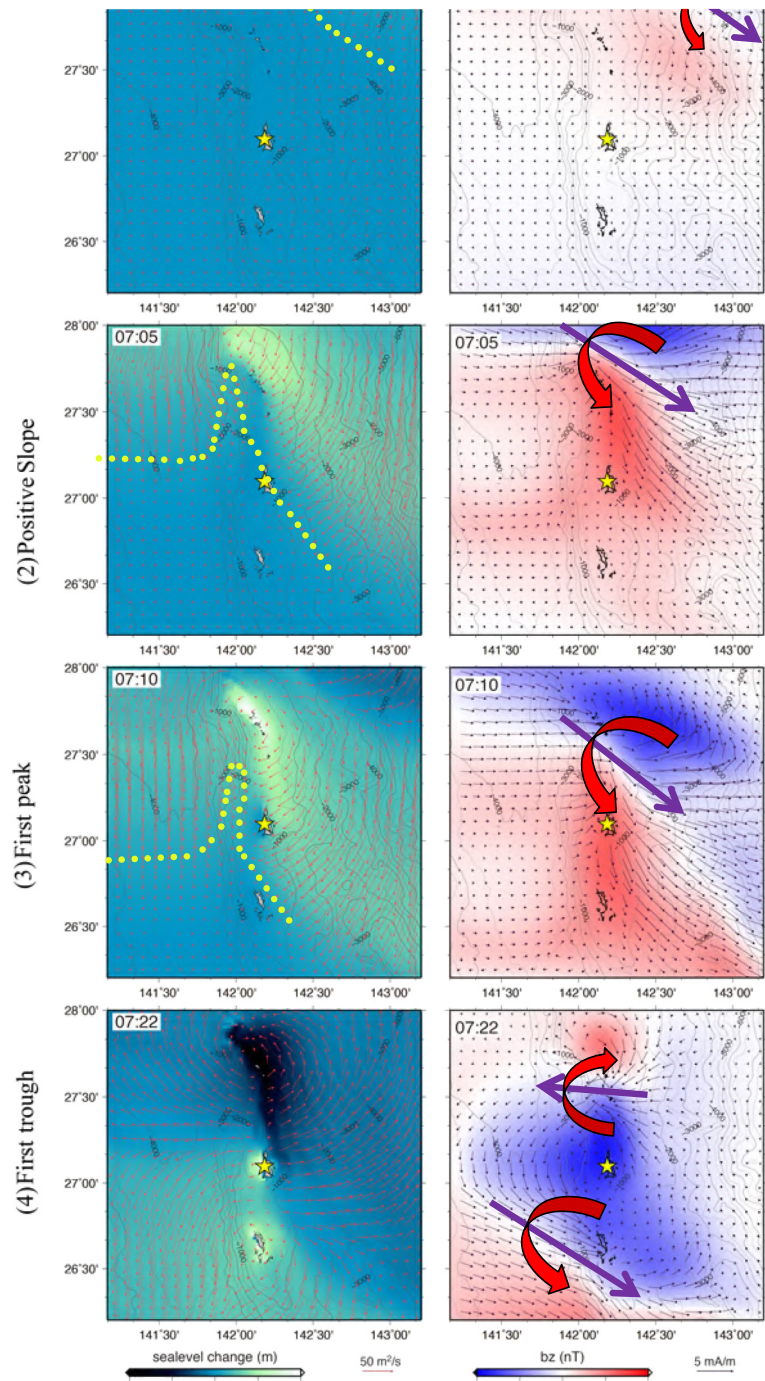
Fig. 7 Simulated tsunami wave height and velocity, and induced electromagnetic field around Chichijima Island (*star*). The *left side* shows wave height and seawater flow (depth-integrated velocity) as color images and vectors, respectively. The *yellow dots* indicate the tsunami fronts. The *right side* shows tsunami-induced magnetic and electric fields as color images and vectors, respectively. The *labels* on the *left side* indicate the phases of magnetic field variations. The *large arrows* indicate representative induced electric currents (*purple vectors*) and secondary induced magnetic fields (*red arcs*)

Tatehata *et al. Earth, Planets and Space* (2015) 67:185

Page 7 of 11

and the first trough (7:22 UTC) is explained as follows.

1 First motion
   The flow of the first tsunami wave was more than 100 km northeast of Chichijima Island. Simultaneously, a weak induced magnetic field extended to Chichijima Island.

2 Positive slope
   The first tsunami wave was northeast of Chichijima Island. Positive and negative variations of the magnetic field were south (front) and farther north (back) of the tsunami wave, respectively.

3 First peak
   The first tsunami wave was near the east coast of Chichijima Island. Induced electric currents near the island flowed from the north to the east. A positive variation of the magnetic field lay over the island, and the following negative variation moved south into the area shown in Fig. 7.

4 First trough
   The first trough of the tsunami reached the northern side of Chichijima Island, and rip flows of the tsunami moved away from the island. A negative variation of the magnetic field lay over the island, and a new positive variation entered the area shown in Fig. 7, moving south.

Equation 14 indicates that an induced electric current is delayed when a tsunami wave is in a phase with the positive slope, but the phase-delay effect of the C_d/C term becomes weak as ocean depth decreases. As such, the induced electric current near the coastline is substantially in phase with the tsunami. Minami et al. (2015) discussed these phenomena in detail.

The first tsunami wave approaching Chichijima Island from the northeast induced an electric current in the leftward direction relative to the tsunami propagation. Around 7:05–7:10, northeast of Chichijima Island, there were large and parallel electric currents (purple arrows in Fig. 7). According to Ampere's right-hand rule, these currents induced large magnetic fields (red arcs in Fig. 7).

From this exercise, we conclude the following: if a tsunami wave is approximately planar, the lines representing the induced electric current and the peak of the tsunami wave are parallel and coincident, and thus, the induced magnetic field must curl over both the electric current and the tsunami wave. Because this induced magnetic field can reach beyond the tsunami wave, its signal precedes the wave and can be detected at least several minutes before the tsunami's arrival.

The amplitudes of the induced magnetic field and the tsunami's height are related with an approximate ratio of 1 nT/m. Four other examples of induced magnetic phenomena recorded at CBI had similar ratios (Tatehata 2015). This sensitivity is sufficient for detecting tsunamis with height of above 1 m, considering the typical signal-to-noise ratio of geomagnetic observations. Our findings suggest the possibility that magnetic field observations can serve as a method for rapid detection of imminent tsunamis.

Conclusion
We showed that the vertical component of the geomagnetic field and the tide gauge records at Chichijima Island exhibited very similar patterns as the tsunami caused by the 2011 Tohoku earthquake. The first magnetic signal preceded the arrival of the first tsunami wave at the Chichijima Island tide gauge by about 20 min.

We quantitatively modeled the tsunami and the corresponding magnetic field variations at Chichijima Island. Not only was the computed magnetic field signal in close agreement with the observed signal, but also the mechanism before the arrival of the tsunami wave was quantitatively explained. Our numerical simulation showed that the straight-line electric current induced a secondary magnetic field that curled at the front of the first tsunami wave.

Appendix 1
Effect of external geomagnetic disturbance
Due to external sources, the horizontal component H of the geomagnetic field induces the vertical component Z depending on the lateral resistivity gradient in the subsurface. The transfer function of $\mathbf{T}$ between horizontal H and vertical Z magnetic components is

$$Z = \mathbf{T}H \tag{2}$$

where $\mathbf{T}$ is a complex number. The amplitude of $\mathbf{T}$ at stations KNY and CBI estimated from Eq. 2 is >0.40 and <0.15, respectively, in the period band between 1000 and 10,000 s (Additional file 1: Figure S1). This indicates that Z induced during geomagnetic storms should be relatively large at KNY, but relatively small at CBI.

Sounding curves of geomagnetic transfer functions ($\mathbf{T}$) at stations CBI and KNY determined using the BIRRP program (Chave and Thomson 2004).

The long-period soundings (320–61,440 s) were estimated from geomagnetic records between 1 April and 30 July 2010. We used the remote reference technique (Gamble et al. 1979) with the data from CBI and KNY for the long-period sounding of KNY and CBI, respectively. The short-period soundings (5.33–256 s) were estimated from the records between 8 and 10 March 2011.

Tatehata *et al. Earth, Planets and Space* (2015) 67:185

Page 8 of 11

A weak geomagnetic storm was observed on 11 March 2011 (Japan Meteorological Agency 2013), and significant variations of H were observed at CBI and KNY (Fig. 3). The strong correlation between Z and H indicates that an external geomagnetic disturbance induced Z at KNY, as the relatively high value of **T** implies. On the other hand, the small value of **T** for CBI does not explain the amplitude of Z between 7:00 and 10:00 (UTC). In addition, H and Z did not appear to be correlated during this period.

To evaluate the effect of the external disturbance on Z at CBI quantitatively, we computed Z from the estimated **T** and the observed H using Eq. 2. The computed Z waveform closely matched the observed data until 7:00, when large oscillations were observed (Additional file 2: Figure S2). Thus, secondary geomagnetic variations of external origin accounted for the observations before 7:00 but not after 7:00.

Appendix 2
Tsunami simulation
To simulate the tsunami around Chichijima Island, we used the following numerical tsunami model, which uses the long-wave approximation and takes into account the shallow bottom friction:

$$\frac{\partial Q_\phi}{\partial t} = -gh\frac{1}{R\cos\lambda}\frac{\partial \eta}{\partial \phi} - \frac{1}{h}\left\{ Q_\phi \frac{1}{R\cos\lambda}\frac{\partial Q_\phi}{\partial \phi} + Q_\lambda \frac{\partial Q_\phi}{\partial \lambda}\right\}$$
$$-\gamma\frac{1}{h^2}Q_\phi\sqrt{Q_\phi{}^2 + Q_\lambda{}^2} - f\,Q_\lambda$$

$$\frac{\partial Q_\lambda}{\partial t} = -gh\frac{1}{R\cos\lambda}\frac{\partial \eta}{\partial \phi} - \frac{1}{h}\left\{ Q_\phi \frac{1}{R\cos\lambda}\frac{\partial Q_\lambda}{\partial \phi} + Q_\lambda \frac{\partial Q_\lambda}{\partial \lambda}\right\}$$
$$-\gamma\frac{1}{h^2}Q_\lambda\sqrt{Q_\phi{}^2 + Q_\lambda{}^2} + f\,Q_\phi$$

$$\frac{\partial \eta}{\partial t} = -\left\{ \frac{1}{R\cos\lambda}\frac{\partial Q_\phi}{\partial \phi} + \frac{\partial Q_\lambda}{\partial y}\right\}, \tag{3}$$

where R is the Earth's radius, λ is the latitude, ϕ is the longitude, h is the water depth, g is the gravity, γ is the friction coefficient of the seabed, f is the Coriolis coefficient, and η is the uplift of the sea surface. Q_ϕ and Q_λ denote vertically integrated flow rates, which are used for the computation of induced electric currents. In this simulation, we used a 1-arcmin-resolution numerical model and the bathymetry dataset ETOPO1 (National Geophysical Data Center).

In numerical simulations of tsunamis, fault models with multiple small active segments are used to produce the initial tsunami wave. For example, Maeda et al. (2011) used 12 small faults, and Satake et al. (2013) used 55 small faults. However, we devised a simple fault model for the purpose described in the main text. In accordance with the Chichijima tide record and DART

buoys located south of the island, arrival times, amplitude, period, and the shape of the tsunami wave were simulated. Finally, we obtained a single simple fault model, centered at 37.88° N, 143.23° E, with the following parameters: strike 203°, length 186 km, width 129 km, slip 25 m, dip angle 16°, slip angle 101°, depth 5.1 km, and slip time function 180 s. The initial uplift of the sea surface from this fault model is shown in Additional file 3: Figure S3.

The resulting computed and observed tsunami waveforms at six DART buoys in the western Pacific Ocean are shown in Additional file 4: Figure S4. The computed waveforms at the Chichijima tide station (Fig. 4), DART 52403, and DART 52405 in the "South Area" (Additional file 4: Figure S4) show good agreement with the observations. Hence, this computation has sufficient accuracy to model the tsunami flow (Q_ϕ, Q_λ) passing through the Chichijima Island area.

Appendix 3
Derivation of the formulae
The induced magnetic field equation of a conductor is represented as

$$\frac{\partial \boldsymbol{B}}{\partial t} = \nabla \times (\boldsymbol{u} \times \boldsymbol{B}) - \nabla \times (K\nabla \times \boldsymbol{B}), \tag{4}$$

where K is the magnetic diffusivity, u is the flow velocity vector of seawater, and B is the magnetic field. The magnetic field B can be decomposed to $B = F + b$, where F is the geomagnetic field and b is the induced magnetic field.

In a homogeneous conductor, the induction equation for the vertical component b_z is

$$\frac{\partial b_z}{\partial t} = -\nabla_H \cdot (F_z \boldsymbol{u_H}) + K\nabla^2 b_z \tag{5}$$

The derivation of Eq. 5 is detailed in Tyler (2005) and Ichihara et al. (2013).

The general solution for Eq. 5 is expressed in the following form, in which the coefficient constants D_1, D_2 are determined by boundary conditions:

$$b_z = -\frac{1}{2\alpha^2 K}\nabla_H \cdot (F_Z \boldsymbol{u_H})[D_1 e^{\alpha x} + D_2 e^{-\alpha x} + 2], \tag{6}$$

where $\alpha := \sqrt{\kappa^2 - i\omega/K}$, ω is the frequency, κ is the wavenumber vector describing the horizontal variation, and x is the position vector, signifying a uniform plane wave.

From Maxwell's equations, the horizontal component b_H of the tsunami propagation direction is expressed as

$$b_H = -\frac{1}{i\kappa}\frac{\partial b_z}{\partial z}$$
$$= -\frac{i}{2\alpha\kappa K}\nabla_H\cdot(F_z\boldsymbol{u}_H)[D_1 e^{\alpha z}-D_2 e^{-\alpha z}]. \quad (7)$$

The boundary conditions for seawater are that b_z and $\partial b_z/\partial z$ are continuous at the upper (sea surface) and lower (seabed) boundaries. The latter condition means that the horizontal component of the magnetic field is continuous at the boundary.

For the coordinate system, the z-direction is perpendicular to the sea surface, $z=0$ is the sea surface, and $z=-h$ is the seabed (h is water the depth). The x-direction is to the east and the y-direction is to the north. In the air above the sea surface and the crust below the seabed, $\nabla^2 b_z=0$.

Then the boundary condition Eq. 7 is reduced as follows:

$$\frac{\partial^2}{\partial z^2}b_z-\kappa^2 b_z=0.$$

In addition, there are other boundary conditions for which the solutions converge to zero at infinite distances from the seawater:

$$b_z = P\,e^{-\kappa z} \quad (0\le z)\,, \quad b_z = Q\,e^{\kappa(z+h)} \quad (z\le-h).$$

From Eqs. 6 and 7 and the boundary conditions, the coefficients D_1, D_2, P, and Q are obtained as

$$D_1 = -\frac{\kappa e^{\frac{\alpha h}{2}}}{\kappa\cosh\frac{\alpha h}{2}+\alpha\sinh\frac{\alpha h}{2}}, \quad D_2 = -\frac{\kappa e^{\frac{-\alpha h}{2}}}{\kappa\cosh\frac{\alpha h}{2}+\alpha\sinh\frac{\alpha h}{2}},$$

$$P = \frac{-1}{\alpha K}\nabla_H\cdot(F_z\boldsymbol{u}_H)\frac{\sinh\frac{\alpha h}{2}}{\kappa\cosh\frac{\alpha h}{2}+\alpha\sinh\frac{\alpha h}{2}},$$

$$Q = \frac{-1}{\alpha K}\nabla_H\cdot(F_z\boldsymbol{u}_H)\frac{\sinh\frac{\alpha h}{2}}{\kappa\cosh\frac{\alpha h}{2}+\alpha\sinh\frac{\alpha h}{2}}.$$

Therefore, Eq. 6 can be rewritten as

$$b_Z = \frac{-1}{\alpha^2 K}\nabla_H\cdot(F_z\boldsymbol{u}_H)\left[1-\frac{\sinh\alpha\left(z+\frac{h}{2}\right)}{\kappa\cosh\frac{\alpha h}{2}+\alpha\sinh\frac{\alpha h}{2}}\right]. \quad (8)$$

Equation 8 is differentiated to obtain

$$\frac{\partial b_Z}{\partial z} = \frac{\kappa}{\alpha K}\nabla_H\cdot(F_z\boldsymbol{u}_H)\left[1-\frac{\sinh\alpha\left(z+\frac{h}{2}\right)}{\kappa\cosh\frac{\alpha h}{2}+\alpha\sinh\frac{\alpha h}{2}}\right]. \quad (9)$$

Moreover, b_H is obtained by rewriting Eq. 7:

$$b_H = \frac{i}{\alpha K}\nabla_H\cdot(F_z\boldsymbol{u}_H)\frac{\sinh\alpha\left(z+\frac{h}{2}\right)}{\kappa\cosh\frac{\alpha h}{2}+\alpha\sinh\frac{\alpha h}{2}}. \quad (10)$$

As the next step, we obtained the electric current in the seawater flow arising from the induced magnetic field b. Using the Maxwell equation for current density j, this electric current is determined by

$$\mu\boldsymbol{j} = \nabla\times\boldsymbol{b},$$

where μ is the magnetic permeability and j is the vector of current density.

Assuming a plane wave solution with wavenumber κ, the magnetic field vector b is decomposed as

$$b_x = \frac{\kappa_x}{\kappa}b_H, \quad b_y = \frac{\kappa_y}{\kappa}b_H.$$

Then, $\mu\boldsymbol{j}$ is described as

$$\mu j_x = i\kappa_y b_z-\frac{\kappa_y}{\kappa}\frac{\partial b_H}{\partial z} = -\frac{\kappa_y}{\kappa}\left(-i\kappa b_z+\frac{\partial b_H}{\partial z}\right),$$
$$\mu j_y = i\kappa_x b_z-\frac{\kappa_x}{\kappa}\frac{\partial b_H}{\partial z} = -\frac{\kappa_x}{\kappa}\left(-i\kappa b_z+\frac{\partial b_H}{\partial z}\right),$$
$$\mu j_x = i\kappa_x b_y-i\kappa_y b_x = i\kappa_x\frac{\kappa_y}{\kappa}b_H-i\kappa_y\frac{\kappa_x}{\kappa}b_H = 0.$$

That is, the current density in the direction perpendicular to the propagation of the tsunami is

$$\mu j_\perp = -i\kappa b_z+\frac{\partial b_H}{\partial z}\ . \quad (11)$$

To compute the induced magnetic field at the Chichijima geomagnetic observatory, we require the total amount of current at density $J_\perp$ in seawater, which is obtained by integrating Eq. 11 from the seabed to the sea surface. Hence,

$$\mu J_\perp = -i\kappa\int_{-h}^{0}b_z dz+b_H|_{-h}^{0} \quad (12)$$

is the integral equation to be solved. Using Eqs. 6 and 7, the terms on the right side of Eq. 12 can be rewritten as

$$i\kappa\int_{-h}^{0}b_z dz = \frac{i\kappa}{2\alpha^2 K}\nabla_H\cdot(F_z u_H)\{2h+\frac{1}{\alpha}(D_1-D_1)$$
$$-\frac{1}{\alpha}\left(D_1 e^{-\alpha h}-D_1 e^{\alpha h}\right)\},$$

and

$$b_H(z=0) = -\frac{i}{2\alpha\kappa K}\nabla_H\cdot(F_z\boldsymbol{u}_H)[D_1-D_2],$$
$$b_H(z=-h) = -\frac{i}{2\alpha\kappa K}\nabla_H\cdot(F_z\boldsymbol{u}_H)\left[D_1 e^{-\alpha h}-D_2 e^{\alpha h}\right].$$

Therefore, the total electric current is

Tatehata *et al. Earth, Planets and Space* (2015) 67:185

Page 10 of 11

$$\mu J_\perp = -\frac{i}{\alpha^2 K}\nabla_H\cdot(F_z\boldsymbol{u}_H)$$

$$\left\{\kappa h + 2\left(1-\frac{\kappa^2}{\alpha^2}\right)\frac{\sinh\alpha h + \frac{\kappa}{\alpha}(\cosh\alpha h - 1)}{\left\{\left(\frac{\kappa}{\alpha}\right)^2 + 1\right\}\sinh\alpha h + 2\frac{\kappa}{\alpha}\cosh\alpha h}\right\}. \tag{13}$$

Here, we use the continuity equation of the tsunami and the long-wave approximation ($u_z \ll |\boldsymbol{u}_H|$) to simplify the flow rate divergence equation by using the height η of the tsunami:

$$\frac{\partial\eta}{\partial t} + \nabla\cdot(h\boldsymbol{u}_H) = 0,$$
$$\nabla_H\cdot(F_z\boldsymbol{u}_H) = \frac{i\omega\eta F_z}{h}.$$

Using the approximation $h \ll \lambda$, Eq. 13 can be rewritten as

$$\mu J_\perp = -\frac{\omega}{\alpha^2 K}\frac{\eta F_z}{h}\left\{\frac{2\sinh\alpha h}{\left\{\left(\frac{\kappa}{\alpha}\right)^2 + 1\right\}\sinh\alpha h + 2\frac{\kappa}{\alpha}\cosh\alpha h}\right\}.$$

Using skin depth $\left(\delta := \sqrt{2K/\omega}\right)$ and the approximation $\delta \ll \lambda$, $\mu J_\perp$ can be further simplified:

$$\mu J_\perp \approx \frac{-\omega}{K}\frac{\eta F_z}{h}\left\{\frac{2}{-2i\frac{1}{\delta^2} + 2\frac{\kappa}{h}}\right\} = -\frac{\eta F_z}{h}\left\{\frac{2}{-i + \frac{2K}{hC}}\right\}.$$

Therefore,

$$\mu J_\perp = -\frac{2i}{1 - iC_d/C}\frac{\eta F_z}{h} \tag{14}$$

is obtained, where $C_d := 2K/h$ and $C := \sqrt{gh}$. This formulation uses only the approximations $h \ll \lambda$ and $\delta \ll \lambda$, and does not use $h \ll \delta$. Hence, Eq. 14 can be applied to tsunamis deeper than the skin depth. The direction of the electric current is estimated by computing the flow velocity vectors.

This derivation assumed that the electrical conductivity of the seafloor is zero. Ichihara et al. (2013), Sugioka et al. (2014), and Minami et al. (2015) described a more extended formulation using a seafloor with finite electrical conductivity. Zhang et al. (2014b) considered the electrical conductivity of the seafloor as a three-dimensional multi-layer structure. However, Tada et al. (2014) showed that the electrical conductivity of the seafloor is less than 0.1 S∕m around Chichijima Island. Hence, the conductivity of the sea floor can be approximated to zero.

Additional files

Additional file 1: Figure S1. Sounding curves of geomagnetic transfer functions (**T**) at stations CBI and KNY determined using the BIRRP program (Chave and Thomson 2004). (PDF 56 kb)

Additional file 2: Figure S2. Observed geomagnetic waveform and computed Z at CBI. (GIF 15,148 kb)

Additional file 3: Figure S3. Results of the fault displacement model (initial tsunami wave) showing the vertical movement of the crust. (PDF 27 kb)

Additional file 4: Figure S4. Map showing tsunami propagation along with DART buoys (yellow squares) and their observed and computed sea-level waveforms (dark and light blue lines, respectively). Tsunami travel times were obtained from NOAA; the contour interval is 1 h. The measurement for DART buoys (red squares; 5204 and 52401) was omitted. (PDF 421 kb)

Author details
[1]Kakioka Magnetic Observatory, Japan Meteorological Agency, 595 Kakioka, Ishioka-shi, Ibaraki-ken 315-0116, Japan. [2]Research and Development Center for Earthquake and Tsunami, Japan Agency for Marine-Earth Science and Technology, 2-15 Natsushima-cho, Yokosuka 237-0061, Japan. [3]Graduate School of Maritime Sciences, Kobe University, 5-1-1 Fukae-minamimachi, Higashinada-ku, Kobe 658-0022, Japan. [4]Department of Deep Earth Structure and Dynamics Research, Japan Agency for Marine-Earth Science and Technology, 2-15 Natsushima-cho, Yokosuka 237-0061, Japan.

References

Chave AD, Thomson DJ (2004) Bounded influence magnetotelluric response function estimation. Geophys J Int 157:988–1006. doi:10.1111/J.1365-246x.2004.02203.X

Faraday M (1832) The Bakerian lecture: experimental researches in electricity—second series. Philos Trans R Soc London 122:163–194. doi:10.1098/rstl.1832.0007

Gamble TD, Clarke J, Goubau WM (1979) Magnetotellurics with a remote magnetic reference. Geophysics 44:53–68

Ichihara H, Hamano Y, Baba K, Kasaya T (2013) Tsunami source of the 2011 Tohoku earthquake detected by an ocean-bottom magnetometer. Earth Planet Sc Lett 382:117–124

Japan Meteorological Agency (2013) Report of the Kakioka Magnetic Observatory 2011, CD-ROM

Maeda T, Furumura T, Sakai S, Shinohara M (2011) Significant tsunami observed at ocean-bottom pressure gauges during the 2011 Off the Pacific Coast of Tohoku earthquake. Earth Planets Space 63(7):803–808

Tatehata *et al. Earth, Planets and Space* (2015) 67:185

Page 11 of 11

Manoj C (2011) Observation of magnetic fields generated by tsunamis. Eos 92:13–14

Minami T, Toh H, Tyler H (2015) Properties of electromagnetic fields generated by tsunami first arrivals: classification based on the ocean depth. Geophys Res Let. doi:10.1002/2015GL063005

Sanford TB (1971) Motionally induced electric and magnetic fields in the sea. J Geophys Res 76:3476–3492. doi:10.1029/JC076i015p03476

Satake K, Fujii F, Harada T, Namegaya Y (2013) Time and space distribution of coseismic slip of the 2011 Tohoku Earthquake as inferred from tsunami waveform data. Bul Seism Soc Am 103(2B):1473–1492. doi:10.1785/0120120122, 2013

Sugioka H, Hamano Y, Baba K, Kasaya T, Tada N, Suetsugu D (2014) Tsunami: ocean dynamo generator. Scientific Reports 4:3596. doi:10.1038/srep03596

Tada N, Baba K, Utada H (2014) Three-dimensional inversion of seafloor magnetotelluric data collected in the Philippine Sea and the western margin of the northwest Pacific Ocean. Geochem Geophys Geosyst 15:2895–2917. doi:10.1002/2014GC005421

Tatehata H (2015) Tsunami-induced magnetic field records at the Chichijima Island observation station. Tech Rep Kakioka Magnetic Obs 12(1–2):11–19 (in Japanese)

Toh H, Satake K, Hamano Y, Fujii Y, Goto T (2011) Tsunami signals from the 2006 and 2007 Kuril earthquakes detected at a seafloor geomagnetic observatory. J Geophys Res 116, B02104. doi:10.1029/2010JB007873

Tyler RH (2005) A simple formula for estimating the magnetic fields generated by tsunami flow. Geophys Res Let 32, L09608. doi:10.1029/2005GL022429

Tyler RH, Maus S, Luhr H (2003) Satellite observations of magnetic fields due to ocean tidal flow. Science 299:239–241. doi:10.1126/science.1078074

Zhang LL, Baba K, Liang PF, Shimizu H, Utada H (2014a) The 2011 Tohoku tsunami observed by an array of ocean bottom electro magnetometers. Geophys Res Lett 41(14):4937–4944. doi:10.1002/2014gl060850

Zhang LL, Utada H, Shimizu H, Baba K, Maeda T (2014b) Three-dimensional simulation of the electromagnetic fields induced by the 2011 Tohoku tsunami. J Geophys Res 119(1):150–168. doi:10.1002/2013jb010264